Pergamon

Int. J. Heat Mass Transfer. Vol. 38, No. 12, pp. 2143–2157, 1995

0017-9310/95 $9.50+0.00

0017-9310(94)00348-3

Stability of natural convection flow in a tall vertical enclosure under non-Boussinesq conditions

S. A. SUSLOV and S. PAOLUCCI†

Department of Aerospace and Mechanical Engineering, University of Notre Dame, Notre Dame, IN 46556, U.S.A.

(*Received* 13 *June* 1994 *and in final form* 6 *November*)

Abstract—We have examined the linear stability of the fully developed natural convection flow in a differentially heated tall vertical enclosure under non-Boussinesq conditions. The three-dimensional analysis of the stability problem was reduced to a two-dimensional one by the use of Squire's theorem. The resulting eigenvalue problem was solved using an integral Chebyshev collocation method. The influence of non-Boussinesq effects on the stability was studied. We have investigated the dependence of the critical Rayleigh number on the temperature difference. The results show that two different modes of instability are possible, one of which is new and due entirely to non-Boussinesq effects. Both types of instability are oscillatory, and the critical disturbance wave speed is zero only in the Boussinesq limit.

1. INTRODUCTION

We study the convection flow in a tall vertical enclosure whose left and right walls are differentially heated. This type of flow is a problem of considerable interest and is frequently encountered in applications such as thermal insulation systems, heat exchangers, electronic equipment, and nuclear reactors. In many such applications, density (or temperature) differences are so large that non-Boussinesq conditions prevail.

The objective of the present work is to examine the linear stability of convection flow in a differentially heated tall vertical cavity under non-Boussinesq conditions. Solution of the Boussinesq equations is generally preferred since they are much simpler in their form. Unfortunately, in many of the applications cited above, density variations can be extremely large: thus the Boussinesq approximation is not applicable.

There are a number of published studies that are related to the present investigation. To gain a better perspective of results to be presented, we summarize their primary conclusions.

In the limiting case of small temperature difference, the flow coincides with that of pure natural convection in a tall open channel since, due to the central symmetry of the velocity profile, the mass flux in each horizontal section is zero for both cases. The stability of this flow in the Boussinesq limit has been analyzed by a number of investigators [1–7]. The major conclusions are that for Prandtl numbers less that 12.45 the instability is shear driven and stationary, and the Prandtl number dependence is slight. The instability is one in which the disturbance energy is gained from the action of the shear forces in the mean flow resulting from natural convection. For $Pr = 0.71$ the critical Rayleigh and wave numbers are found to be $Ra_c^0 = 5706.27$ and $\alpha_c^0 = 2.8$. For Prandtl numbers larger that 12.45, the instability is thermally driven and oscillatory. The instability in this case is one in which the disturbance energy is gathered primarily from the potential energy associated with the buoyant forces.

Recently, Suslov and Paolucci [8] showed that, when properties are allowed to vary (non-Boussinesq case), the solutions for the basic flow are different for open and closed cavity cases, since due to the asymmetry of the velocity profile the net mass flux is not necessarily zero for the open channel. Thus the stability problem for the closed cavity flow under non-Boussinesq conditions requires a separate analysis.

Taking into account only viscosity variations for the flow within a tall but closed cavity, Thangam and Chen [9] and Chen and Pearlstein [7] find that the instability is always oscillatory for arbitrary values of Prandtl number. No quantitative information regarding wave speeds is given.

The present paper is organized as follows. First we formulate the problem to be studied. This is followed by a description of the basic flow which is an exact solution of the problem. We next formulate the linear stability problem of this flow, and subsequently solve the resulting perturbation equations using an integral Chebyshev collocation method. The primary conclusions of the study, for air as the working fluid, are that: (i) the instability is always oscillatory; (ii) for temperature differences smaller than a critical value, the instability is always shear driven and (iii) for temperature differences greater than the critical value, a

†Author to whom correspondence should be addressed.

NOMENCLATURE

A_H, A_D height to width and depth to width aspect ratios
c wave speed
c_p, c_v specific heats at constant pressure and constant volume
D enclosure depth; differential operator
E_{KE}, E_{PE} disturbance kinetic and thermal potential energy
g absolute value of the gravity force
Gr Grashof number
H enclosure height
k thermal conductivity
L enclosure width
n_i unit vector in direction of gravity force
N number of collocation points
P thermodynamic pressure
Pr Prandtl number
Ra Rayleigh number
S_μ, S_k Sutherland constants
t time
T temperature
ΔT temperature difference
u_i, (u, v, w) velocity components
W_{ij} discrete integral operator
x_i, (x, y, z) spatial coordinates
$\hat{x}$ transformed x-coordinate.

Greek symbols

α thermal diffusivity; longitudinal wave number
β thermal expansion coefficient
γ ratio of specific heats; transverse wave number
Γ fluid resilience parameter
δ_{ij} Kronecker delta
ε dimensionless temperature difference
κ isothermal compressibility coefficient
λ bulk viscosity; dynamic pressure gradient parameter
μ dynamic viscosity
ν kinematic viscosity
Π hydrodynamic/hydrostatic pressure
ρ density
σ coefficient of tension; complex amplification rate
τ_{ij} shear stress tensor.

Subscripts

c evaluated at cold temperature; critical value
h evaluated at hot temperature
I imaginary part
r evaluated at reference conditions
R real part.

Superscripts

0 point on marginal stability curve
$'$ disturbance quantity
$*$ dimensional quantity
$\bar{}$ basic flow quantity
$\hat{}$ disturbance amplitude
$\tilde{}$ transformed quantity.

new mode of instability (due entirely to non-Boussinesq effects) is found which is purely thermal in character in that the disturbance energy is gained from the potential energy associated with the buoyant forces, and is analogous to the type of instability found for $Pr > 12.45$ in the Boussinesq case.

2. PROBLEM FORMULATION

Consider the flow of a fluid in an enclosure having aspect ratios $A_H = H/L$, $A_D = D/L$, where L is the distance between the vertical walls, and H and D are height and depth of the enclosure, respectively. The x^*-coordinate is fixed on the left wall, and the y^*-coordinate is positive in the upwards direction. The left and right walls of the cavity are isothermally heated and cooled, respectively, resulting in a temperature difference $\Delta T = T_h^* - T_c^* > 0$. The other four walls are taken adiabatic. Asterisk superscripts denote dimensional quantities.

We nondimensionalize the problem with reference quantities for length, velocity, temperature and thermodynamic pressure using the enclosure width L, the thermal diffusion speed $u_r = \alpha_r/L$, the average temperature $T_r = (T_h^* + T_c^*)/2$ and the initial pressure $P_r = P_0^*$, respectively. The problem is non-dimensionalized as follows:

$$x_i^* = Lx_i \quad t^* = (L/u_r)t \quad u_i^* = u_r u_i \quad \Pi^* = \rho_r u_r^2 \Pi$$

$$\rho^* = \rho_r \rho \quad T^* = T_r T \quad P^* = P_r P \quad c_p^* = c_{p_r} c_p$$

$$c_v^* = c_{v_r} c_v \quad \beta^* = \beta_r \beta \quad \mu^* = \mu_r \mu \quad \lambda^* = \lambda_r \lambda \quad k^* = k_r k \tag{1}$$

where we have introduced the reference density ρ_r, dynamic viscosity μ_r, bulk viscosity λ_r, thermal conductivity k_r, specific heats at constant pressure and volume c_{p_r} and c_{v_r}, coefficient of thermal expansion β_r, and thermal diffusivity $\alpha_r = k_r/\rho_r c_{p_r}$, all evaluated at the reference temperature and pressure.

The resulting dimensionless governing equations, valid under low Mach number conditions, but allowing for arbitrary density variations, are given as follows (see [10]):

$$\frac{\partial \rho}{\partial t}+\frac{\partial \rho u_i}{\partial x_i}=0, \tag{2}$$

$$\frac{\partial \rho u_i}{\partial t}+\frac{\partial \rho u_j u_i}{\partial x_j}=-\frac{\partial \Pi}{\partial x_i}+\frac{RaPr}{2\varepsilon}(\rho-1)n_i+Pr\frac{\partial \tau_{ij}}{\partial x_j} \tag{3}$$

$$\rho c_p\left(\frac{\partial T}{\partial t}+u_j\frac{\partial T}{\partial x_j}\right)-\Gamma\beta T\frac{dP}{dt}=\frac{\partial}{\partial x_j}\left(k\frac{\partial T}{\partial x_j}\right) \tag{4}$$

$$\rho=\rho(P,T) \tag{5}$$

where $u_i=(u,v,w)$ are velocity components in the $x_i=(x,y,z)$ directions, respectively, $\Pi(x_i,t)=p(x_i,t)-P(t)-(RaPr/2\varepsilon)x_in_i$ is a reduced pressure which accounts for hydrodynamic effects, $n_i=(0,-1,0)$ is the unit vector in the direction of gravity, and τ_{ij} is the viscous stress tensor given by

$$\tau_{ij}=\mu\left(\frac{\partial u_i}{\partial x_j}+\frac{\partial u_j}{\partial x_i}\right)+\lambda\delta_{ij}\frac{\partial u_k}{\partial x_k} \tag{6}$$

where δ_{ij} is the Kronecker delta.

The spatially uniform pressure $P=P(t)$ appearing in the energy equation and the equation of state accounts for the change of static pressure with time. The separation of pressure components in the low Mach number limit is essential in removing acoustic waves from the equations: however, this splitting introduces P as an extra unknown. The general equation of state (5) can be rewritten more explicitly as

$$\rho=\exp\left(-\int_1^T\beta\,dT'+\int_1^P\kappa\,dP'\right) \tag{7}$$

where $\beta=-(\partial\rho/\partial T)_P/\rho$ is the coefficient of volume expansion, and $\kappa=(\partial\rho/\partial P)_T/\rho$ is the isothermal compressibility coefficient. Now using the equation of state (7) and energy equation (4), it can be readily shown that the continuity equation (2) can also be rewritten as

$$\frac{\partial u_i}{\partial x_i}=-\frac{1}{\gamma_r}\frac{\kappa c_v}{c_p}\frac{dP}{dt}+\frac{\beta}{\rho c_p}\frac{\partial}{\partial x_j}\left(k\frac{\partial T}{\partial x_j}\right). \tag{8}$$

Subsequently, integration of (8) over the cavity volume V leads to the following differential–integral equation for the static pressure:

$$\frac{dP}{dt}=\gamma_r\frac{\displaystyle\int_V\frac{\beta}{\rho c_p}\frac{\partial}{\partial x_j}\left(k\frac{\partial T}{\partial x_j}\right)dV}{\displaystyle\int_V\frac{\kappa c_v}{c_p}dV}. \tag{9}$$

This equation is complemented by the initial condition

$$P=1 \quad \text{at } t=0. \tag{10}$$

The independent dimensionless parameters appearing in the equations are respectively the Rayleigh number, the temperature difference, the Prandtl number, and a measure of fluid resilience:

$$Ra=\frac{\beta_r g\Delta T L^3}{\nu_r\alpha_r} \quad \varepsilon=\tfrac{1}{2}\beta_r\Delta T \quad Pr=\frac{\nu_r}{\alpha_r}$$

$$\Gamma=\frac{1}{\sigma_r T_r}\left(\frac{\gamma_r-1}{\gamma_r}\right). \tag{11}$$

In the above definitions g is the magnitude of the gravitational field, and $\nu_r=\mu_r/\rho_r$ is the kinematic viscosity, $\gamma_r=c_{p_r}/c_{v_r}$ is the ratio of specific heats and $\sigma_r=(\partial P/\partial T)_\rho/P|_r$ is the coefficient of tension, all evaluated at the reference temperature.

We emphasize the fact that equations (3), (4) and (7)–(9) are applicable to the natural convection flow of any fluid within a fully enclosed cavity. No assumptions regarding property variations are made. Solutions of these equations account for all non-Boussinesq effects in natural convection. Most non-Boussinesq results to date are for air, whose flow may accurately be described by using the Stokes assumption $\lambda=-\frac{2}{3}\mu$ and the thermodynamic properties by the calorically perfect gas assumptions $c_p=1$, $c_v=1$, $\beta=1/T$, $\kappa=1/P$ and $\sigma=1/T$. Subsequently, we have that $\Gamma=(\gamma_r-1)/\gamma_r$ and equations (7)–(9) simplify to

$$\rho=\frac{P}{T} \tag{12}$$

$$P\frac{\partial u_i}{\partial x_i}=-\frac{1}{\gamma_r}\frac{dP}{dt}+\frac{\partial}{\partial x_j}\left(k\frac{\partial T}{\partial x_j}\right) \tag{13}$$

$$\frac{dP}{dt}=\frac{\gamma_r}{V}\int_S k\frac{\partial T}{\partial x_j}dS_j \tag{14}$$

where S is the cavity dimensionless surface area. Alternately, using the equation of state (12) in the global mass conservation statement

$$\frac{d}{dt}\int_V\rho\,dV=0$$

the thermodynamic pressure can be obtained from

$$P(t)=\left(\frac{1}{V}\int_V\frac{1}{T}dV\right)^{-1}. \tag{15}$$

In addition, for air $\gamma_r=7/5$, $Pr=0.71$, and the transport properties are accurately approximated by the Sutherland law models

$$\mu=T^{3/2}\left(\frac{1+S_\mu}{T+S_\mu}\right) \quad k=T^{3/2}\left(\frac{1+S_k}{T+S_k}\right) \tag{16}$$

where, using $T_r=300$ K and normal pressure, the dimensionless Sutherland constants are $S_\mu=S_\mu^*/T_r=0.368$ and $S_k=S_k^*/T_r=0.648$ (see White [11]).

Boundary conditions at the vertical walls are given by

$$u_i=0 \quad T=T_h=1+\varepsilon \quad \text{at } x=0 \tag{17}$$

$$\text{and} \quad u_i=0 \quad T=T_c=1-\varepsilon \quad \text{at } x=1.$$

From the definition of ε we note that $0<\varepsilon<1$ cor-

responds to the dimensional temperature difference range of $0 < \Delta T < \infty$. Obviously the range of validity of the Sutherland law is considerably less. As a point of reference, note that $\varepsilon = 0.6$ corresponds to $T_h^* = 480$ K and $T_c^* = 120$ K for $T_r = 300$ K, and represents a practical upper limit on the validity of the results for air resulting from increasing errors in the Sutherland law conductivity at the cold wall [12]. Finally we note that Paolucci [10] has shown that, in the limit $\varepsilon \to 0$, we have $P = 1$, $dP/dt = 0$, and equations (2)–(5) reduce to the classical Boussinesq equations. It is emphasized that the Boussinesq equations will yield relatively accurate solutions only for small temperature differences. For example, Gray and Giorgini [13] show that the maximum temperature differences for air and water for which the Boussinesq equations are applicable are 28.6 and 1.25°C, respectively.

3. BASIC FLOW

In the region located in the middle part of the enclosure, for large enough aspect ratios $(A_H, A_D) \gg 1$ a fully developed flow can exist $(A_H \gtrsim (2+Ra/400)$ as was shown by Chenoweth and Paolucci [14], and typically $A_D \gtrsim 10$ if walls in the depth direction are adiabatic). For such a flow $\bar{u}_i = (0, \bar{v}(x), 0)$, $\bar{T} = \bar{T}(x)$, $\bar{\Pi} = \bar{\Pi}(y)$ and $\bar{P} = \text{const.}$, so that the steady-state problem reduces to

$$\frac{d}{dx}\left(\bar{\mu}\frac{d\bar{v}}{dx}\right) = \frac{Ra}{2\varepsilon}(\bar{\rho} - \lambda) \tag{18}$$

$$\frac{d}{dx}\left(\bar{k}\frac{d\bar{T}}{dx}\right) = 0 \tag{19}$$

$$\bar{\rho} = \frac{\bar{P}}{\bar{T}} \tag{20}$$

$$\bar{P} = \left(\int_0^1 \frac{1}{\bar{T}}dx\right)^{-1} \tag{21}$$

$$\bar{v} = 0 \quad \bar{T} = T_h = 1+\varepsilon \quad \text{at } x = 0 \tag{22}$$

$$\text{and} \quad \bar{v} = 0 \quad \bar{T} = T_c = 1-\varepsilon \quad \text{at } x = 1$$

where $\lambda \equiv 1 - (2\varepsilon/RaPr)\, d\bar{\Pi}/dy = \text{const.}$ and, using (16), we have $\bar{\mu} = \mu(\bar{T})$ and $\bar{k} = k(\bar{T})$. In addition, taking into account the fact that the total mass flux in every horizontal section must be zero we have the additional implicit integral link to obtain λ:

$$\int_0^1 \bar{\rho}\bar{v}\, dx = 0. \tag{23}$$

The solution of these equations is (see ref. [14])

$$\bar{P} = S_k \frac{f_h - f}{F_h - F_c} \tag{24}$$

$$x = \frac{f_h - f}{f_h - f_c} \tag{25}$$

$$\bar{v} = \frac{Ra}{2\varepsilon}\frac{\delta S_k}{Q^2}\left(\frac{1+S_k}{1+S_\mu}\right) \times \left[\left(\lambda + \frac{\bar{P}}{S_k}\right)(\theta_c\omega - \omega_c\theta) - \lambda(\theta_c\phi - \phi_c\theta)\right] \tag{26}$$

where $f, F, Q, \delta, \theta, \phi, \omega$ are functions of $\bar{T}$ and S_k and are given in Appendix A. The expression for λ, while not given here, can also be written in an explicit form [14]. It can be shown that the solution in the Boussinesq limit ($\varepsilon \ll 1$) to leading order reduces to $\bar{P} = 1$ and

$$\bar{T} = 1 + \varepsilon(1-2x) \tag{27}$$

$$\bar{v} = \frac{Ra}{12}x(1-x)(1-2x). \tag{28}$$

The basic flow solution is displayed in Fig. 1 for several values of ε. From Figs. 1(a) and (b) we see immediately that in general the solution does not have any symmetry with respect to x. Only in the Boussinesq limit is the flow symmetric about $x = 1/2$, but this is not the case when ε is finite due to property variations. In Figs. 1(c) and (d) we show the dependence of the thermodynamic pressure $\bar{P}$ and the scaled hydrodynamic pressure gradient λ on the temperature difference. Both of them decrease for the given range of ε. A more detailed discussion of the basic flow is given by Chenoweth and Paolucci [14].

Alternately, the basic flow solution can be obtained numerically using an integral Chebyshev collocation method [15, 16]. In this case equations (18)–(23) are solved over the domain $\hat{x} \in [-1, 1]$ $(\hat{x} = -1 + 2x)$ for convenience. The method can be described as follows. The discrete integral operator W_{ij} is defined by the following relationship

$$F(\hat{x}) = \int_{-1}^{\hat{x}} f(\xi)\, d\xi \Leftrightarrow F(\hat{x}_i) = \sum_{j=1}^{N+1} W_{ij} f(\hat{x}_j) \tag{29}$$

with collocation points selected at $\hat{x}_i = \cos[\pi(i-1)/N]$, $1 \leqslant i \leqslant N+1$. Then the solution of the problem can be written in the form

$$\bar{T}_i = (1+\varepsilon)e_i - 2\varepsilon \frac{\sum_{j=1}^{N+1} W_{ij}/k(\bar{T}_j)}{\sum_{j=1}^{N+1} W_{ij}/k(\bar{T}_j)} \tag{30}$$

$$\bar{v}_i = \frac{Ra}{8\varepsilon}\sum_{j=1}^{N+1}\frac{W_{ij}}{\mu(\bar{T}_j)}\left\{\sum_{k=1}^{N+1} W_{jk}\left(\frac{\bar{P}}{\bar{T}_k} - \lambda e_k\right) + Ce_j\right\} \tag{31}$$

where $i = 1, \ldots, N+1$, $e_i = 1$,

$$C = -\sum_{j=1}^{N+1}\frac{W_{1j}}{\mu(\bar{T}_j)}\left\{\sum_{k=1}^{N+1} W_{jk}\left(\frac{\bar{P}}{\bar{T}_k} - \lambda e_k\right)\right\} \Bigg/ \sum_{j=1}^{N+1}\frac{W_{1j}}{\mu(\bar{T}_j)} \tag{32}$$

and

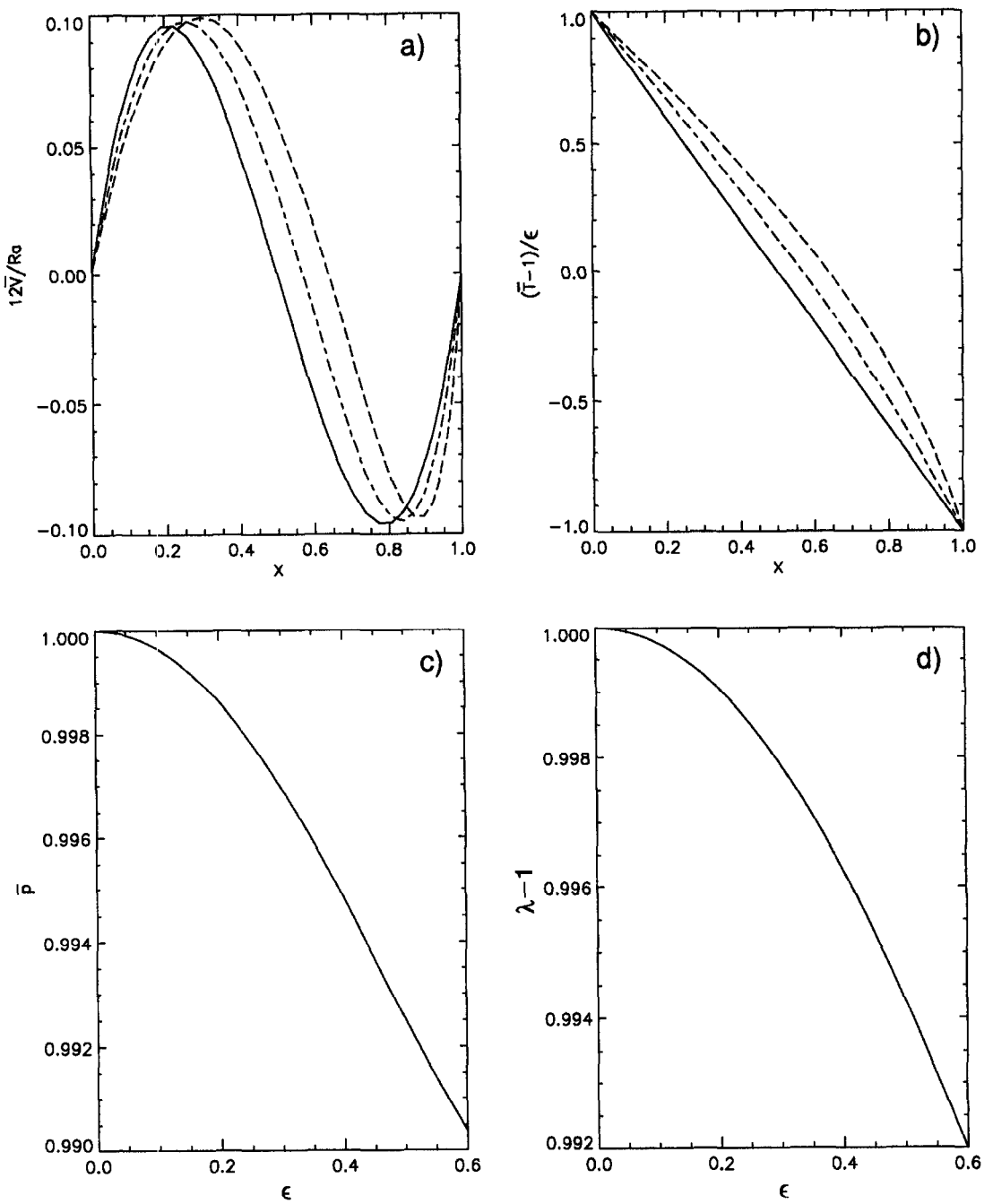

Fig. 1. Basic flow solution: (a) velocity and (b) temperature for $\varepsilon \ll 1$ (——), $\varepsilon = 0.3$ (— — —), $\varepsilon = 0.6$ (- - - -), (c) thermodynamic pressure and (d) hydrodynamic pressure gradient as functions of ε.

$$\bar{P} = \left(\sum_{m=1}^{N+1} \frac{W_{1m}}{\bar{T}_m} \right)^{-1}. \tag{33}$$

The system of nonlinear equations (30) is solved first using the IMSL [17] routine NEQNF. Subsequently, $\bar{P}$ and $\bar{v}_i$ are explicitly evaluated from (33) and (31). Finally, using a simple iterative procedure, λ is found from

$$\sum_{j=1}^{N+1} W_{1j} \frac{\bar{v}_j}{\bar{T}_j} = 0. \tag{34}$$

It should be noticed that, in the Boussinesq limit, since the variation of temperature is small, $\mu(\bar{T})$ and $k(\bar{T})$ reduce to constants equal to unity. Taking into consideration the fact that

$$\sum_{j=1}^{N+1} W_{ij} \hat{x}_j^m = [\hat{x}_i^{m+1} + (-1)^m]/(m+1),$$

the *numerical* solution equations (30) and (31) reduces to the *analytical* solution equations (27) and (28)

evaluated at the collocation points (accounting for the coordinate change):

$$\bar{T}_i = e_i - \varepsilon \hat{x}_i \tag{35}$$

$$\bar{v}_i = \frac{Ra}{48}\hat{x}_i(\hat{x}_i + e_i)(\hat{x}_i - e_i). \tag{36}$$

To ensure the accuracy of the numerical method, the non-Boussinesq numerical results were compared with the analytical solution obtained earlier. It has been shown that the discretization error decays exponentially with increasing number of collocation points [18]. The accuracy of the solution approaches the computer round off error of 10^{-14} when the number of collocation points reaches 22. We note that in reporting all numerical results in the Boussinesq limit of $\varepsilon \ll 1$ we actually use the value of $\varepsilon = 10^{-5}$ for the computations.

4. STABILITY ANALYSIS

We now decompose the dependent variables into two parts, the basic flow and a disturbance:

$$\begin{aligned} u_i &= \bar{u}_i(x) + u_i'(x,y,z,t) \\ \rho &= \bar{\rho}(x) + \rho'(x,y,z,t) \\ \Pi &= \bar{\Pi}(y) + \Pi'(x,y,z,t) \\ T &= \bar{T}(x) + T'(x,y,z,t) \\ P &= \bar{P} + P'(t). \end{aligned} \tag{37}$$

Note that, consistent with the low Mach number approximation, the thermodynamic pressure disturbance P' can depend only on time.

Substituting (37) into equations (3), (4), (6), (12) and (13), substracting the basic flow, and neglecting second order disturbance terms, we obtain the following set of equations for the disturbance quantities:

$$\bar{\rho}\frac{\partial u_j'}{\partial x_j} + \frac{1}{\gamma_r}\frac{dP'}{dt} = \frac{\partial}{\partial x_i}\left(\bar{k}\frac{\partial T'}{\partial x_i} + k'\frac{\partial \bar{T}}{\partial x_i}\right) \tag{38}$$

$$\bar{\rho}\left(\frac{\partial u_i'}{\partial t} + \bar{v}\frac{\partial u_i'}{\partial y} + u'\frac{d\bar{u}_i}{dx}\right) = -\frac{\partial \Pi'}{\partial x_i} + \frac{RaPr}{2\varepsilon}\rho' n_i + Pr\frac{\partial \tau_{ij}'}{\partial x_j} \tag{39}$$

$$\bar{\rho}\left(\frac{\partial T'}{\partial t} + \bar{v}\frac{\partial T'}{\partial y} + u'\frac{d\bar{T}}{dx}\right) - \Gamma\frac{dP'}{dt} = \frac{\partial}{\partial x_i}\left(\bar{k}\frac{\partial T'}{\partial x_i} + k'\frac{\partial \bar{T}}{\partial x_i}\right) \tag{40}$$

$$\frac{\rho'}{\bar{\rho}} = \frac{P'}{\bar{P}} - \frac{T'}{\bar{T}} \tag{41}$$

where

$$\tau_{ij}' = \bar{\mu}\left[\left(\frac{\partial u_i'}{\partial x_j} + \frac{\partial u_j'}{\partial x_i}\right) - \tfrac{2}{3}\delta_{ij}\frac{\partial u_k'}{\partial x_k}\right] + \mu'\left(\frac{\partial \bar{u}_i}{\partial x_j} + \frac{\partial \bar{u}_j}{\partial x_i}\right) \tag{42}$$

and we use the fact that

$$\mu' = \bar{\mu}_T T' \quad k' = \bar{k}_T T'$$

where $\bar{f}_T \equiv \overline{(df/dT)}$. In addition, substituting (37) into (17), we obtain the boundary conditions for the perturbed quantities:

$$u_i' = T' = 0 \quad \text{at } x = 0, 1. \tag{43}$$

Finally, from (15) we obtain

$$P' = \frac{\bar{P}^2}{V}\int_V \frac{T'}{\bar{T}^2}\,dV. \tag{44}$$

Since $(A_H, A_D) \gg 1$, then within the fully developed region we assume periodicity in the y and z directions so that the disturbance quantities (u_i', Π', ρ', T') are of the form $f'(x,y,z,t) = \hat{f}(x)e^{i(\alpha y + \gamma z) + \sigma t}$ and $P'(t) = \hat{P}e^{\sigma t}$, where $\hat{P} = \text{const.}$, α and γ are the longitudinal and transverse real wave numbers, and $\sigma = \sigma_R + i\sigma_I$ is the complex amplification rate. The real and imaginary parts of σ represent the amplification rate of the disturbance and the frequency, respectively. The mode is stable, neutrally stable, or unstable depending on whether σ_R is negative, zero, or positive. Now dropping the hats, and since from (44) we have that

$$P = \begin{cases} \bar{P}^2 \displaystyle\int_0^1 \frac{T(x)}{\bar{T}(x)^2}\,dx & \text{if } \alpha^2 + \gamma^2 = 0 \\ 0 & \text{if } \alpha^2 + \gamma^2 \neq 0 \end{cases} \tag{45}$$

then equations (38)–(41) result in the following system of ordinary differential equations:

$$\bar{P}(Du + i\alpha v + i\gamma w)$$

$$= D(\bar{k}DT + \bar{k}_T D\bar{T}T) - \bar{k}(\alpha^2 + \gamma^2)T - \frac{\sigma}{\gamma_r}P \tag{46}$$

$$[\bar{\rho}(\sigma + i\alpha\bar{v})]u = -D\Pi + Pr\{\tfrac{2}{3}D[\bar{\mu}(2Du - i\alpha v - i\gamma w)]$$

$$-\bar{\mu}[(\alpha^2 + \gamma^2)u - i(\alpha Dv + \gamma Dw)] + i\alpha\bar{\mu}_T D\bar{v}T\} \tag{47}$$

$$[\bar{\rho}(\sigma + i\alpha\bar{v})]v + \bar{\rho}D\bar{v}u$$

$$= -i\alpha\Pi - \frac{RaPr}{2\varepsilon}\rho$$

$$+ Pr\{D[\bar{\mu}(Dv + i\alpha u) + \bar{\mu}_T D\bar{v}T]$$

$$-\bar{\mu}[(\alpha^2 + \gamma^2)v + \tfrac{1}{3}\alpha(2iDu + \alpha v + \gamma w)]\} \tag{48}$$

$$[\bar{\rho}(\sigma + i\alpha\bar{v})]w = -i\gamma\Pi + Pr\{D[\bar{\mu}(Dw + i\gamma u)]$$

$$-\bar{\mu}[(\alpha^2 + \gamma^2)w + \tfrac{1}{3}\gamma(2iDu + \alpha v + \gamma w)]\} \tag{49}$$

$$[\bar{\rho}(\sigma + i\alpha\bar{v})]T + \bar{\rho}D\bar{T}u$$

$$= D(\bar{k}DT + \bar{k}_T D\bar{T}T) - \bar{k}(\alpha^2 + \gamma^2)T + \Gamma\sigma P \tag{50}$$

$$\frac{\rho}{\bar{\rho}} = \frac{P}{\bar{P}} - \frac{T}{\bar{T}} \tag{51}$$

where $D^n = d^n/dx^n$. Equations (45)–(51), together with the boundary conditions

$$u_i = T = 0 \quad \text{at } x = 0, 1 \tag{52}$$

constitute a three-dimensional eigenvalue problem for the complex amplification rate σ.

Using Squire's transformation

$$\tilde{u} = u \quad \tilde{\alpha}\tilde{v} = \alpha v + \gamma w \quad \tilde{w} = w \quad \tilde{T} = T$$
$$\tilde{\rho} = \rho \quad \tilde{P} = P \quad \tilde{\Pi} = \Pi \tag{53}$$
$$\tilde{\alpha}^2 = \alpha^2 + \gamma^2 \quad \tilde{\gamma} = \gamma \quad \tilde{\sigma} = \sigma$$
$$\tilde{Ra} = \frac{\alpha}{\tilde{\alpha}} Ra \quad \tilde{\varepsilon} = \varepsilon \quad \tilde{Pr} = Pr \quad \tilde{\Gamma} = \Gamma$$

it can be easily shown that equations resulting from (45)–(48) and (50), (51) are independent of $\tilde{w}$ and $\tilde{\gamma}$, while that resulting from (49) depends on all variables. Furthermore, if the equation corresponding to (49) is then multiplied by $\tilde{w}^*$ (the complex conjugate of $\tilde{w}$) and integrated by parts over the width of channel, and use a theorem proved by Vasilyev and Paolucci [18], we then obtain that

$$\tilde{\sigma} = \tilde{\sigma}_R + i\tilde{\sigma}_I = -\frac{\langle \tilde{\mu}(|D\tilde{w}|^2 + \tilde{\alpha}^2|\tilde{w}|^2)\rangle}{\langle \tilde{\rho}|\tilde{w}|^2\rangle} - i\tilde{\alpha}\frac{\langle \tilde{\rho}\tilde{v}|\tilde{w}|^2\rangle}{\langle \tilde{\rho}|\tilde{w}|^2\rangle}. \tag{54}$$

Thus the eigenvalue associated with the transverse momentum equation always has a negative real part since $\tilde{\rho} > 0$ and $\tilde{\mu} > 0$. We note then that the reduced eigenvalue problem is identical to the problem obtained without the use of Squire's transformation but with $w = \gamma = 0$. Furthermore, since $\tilde{Ra} \leqslant Ra$, then Squire's theorem holds, so that two-dimensional disturbances are the most unstable. Thus, in presenting all results, we drop the tilde accents reflecting the above finding.

Due to equation (45), the stability calculations for the case where $\alpha = 0$ have been carried out separately. We have found that these disturbances are stable in all cases. Subsequently, the two-dimensional eigenvalue problem can be rewritten in matrix form as:

$$\begin{bmatrix} A_{11} & A_{12} & A_{13} & A_{14} \\ A_{21} & A_{22} & A_{23} & A_{24} \\ A_{31} & 0 & A_{33} & 0 \\ A_{41} & A_{42} & A_{43} & 0 \end{bmatrix} \begin{bmatrix} u \\ v \\ T \\ \Pi \end{bmatrix} = \sigma \begin{bmatrix} 1 & 0 & 0 & 0 \\ 0 & 1 & 0 & 0 \\ 0 & 0 & 1 & 0 \\ 0 & 0 & 0 & 0 \end{bmatrix} \begin{bmatrix} u \\ v \\ T \\ \Pi \end{bmatrix} \tag{55}$$

where A_{ij} are operators defined in Appendix B. Equation (55) together with boundary conditions

$$u = v = T = 0 \quad \text{at } x = 0, 1 \tag{56}$$

defines the two-dimensional complex eigenvalue problem for the amplification rate σ.

As done in the numerical solution of the basic flow, we solve the eigenvalue problem in the domain $\hat{x} \in [-1, 1]$. Using discrete integral and differential operators [15, 16], the eigenvalue problem can be rewritten in discrete form as

$$\mathbf{AX} = \sigma \mathbf{BX}, \tag{57}$$

where

$$\mathbf{X} = (u_1'', \ldots, u_{N+1}'', v_1'', \ldots, v_{N+1}'', T_1'', \ldots, T_{N+1}'', \Pi_1, \ldots, \Pi_{N+1})^T \tag{58}$$

and $\mathbf{A}$ and $\mathbf{B}$ are the $[4(N+1)] \otimes [4(N+1)]$ matrices obtained from collocation discretization of (55). The eigenvalues σ are then obtained using the IMSL [17] routine GVLCG.

For fixed parameters α and ε the values of Ra and σ_I at which $\sigma_R = 0$ are found. Repeating such a procedure for different values of α and the same ε, we obtain the marginal stability curve, say $Ra_m(\alpha, \varepsilon)$ and the corresponding frequency $\sigma_{Im}(\alpha, \varepsilon)$. Critical values $Ra_c(\alpha_c, \varepsilon) = \min_{\alpha} Ra_m(\alpha, \varepsilon)$ and $\sigma_{I_c}(\varepsilon) = \sigma_{I_m}(\alpha_c, \varepsilon)$, and thus also the critical wavespeed $c_c = -\sigma_{I_c}/\alpha_c$ are then obtained for different values of $\varepsilon \in (0, 0.6]$. Results of these calculations using the above procedure and the previously noted parameter values appropriate for air are presented next. In addition, all results have been obtained using 39 Chebyshev modes, and all values are believed to be correct to the significant figures reported.

5. RESULTS

In Fig. 2 we show marginal stability curves and critical parameters as functions of ε. From the marginal stability curves shown in Fig. 2(a) we see that as the temperature difference parameter is increased, at first the only effect appears to be a shift of the marginal curve to higher values of Rayleigh numbers. This leads to larger values of Ra_c as shown in Fig. 2(b). For the temperature difference parameter range of $0 < \varepsilon \leqslant \varepsilon_*$, where $\varepsilon_* = 0.536$, the critical Rayleigh number can be well approximated by $Ra_c/Ra_c^0 = 1 + 1.450\varepsilon^2 + 2.914\varepsilon^4$, where $Ra_c^0 = 5706.6927$. Note that the value of $Ra_c^0/Pr = 8037.5944$ coincides with Gr_c^0 given in [8], where Gr_c^0 is the Boussinesq limit critical Grashof number for the flow in a tall open vertical channel. This fact shows that in the Boussinesq limit, the natural convection flows for closed and open tall vertical channels are similar. In contrast, in the non-Boussinesq regime the flow in a closed cavity is more stable than one in an open channel [8].

The increase of Ra_c with ε is accompanied by a slight decrease in the critical wavenumber α_c from the value of $\alpha_c^0 = 2.810$ in the Boussinesq limit as shown in Fig. 2(c). One important point to note, which can be seen from Fig. 2(d), is that the critical wave speed is zero *only* in the Boussinesq limit. For the range $0 < \varepsilon \leqslant \varepsilon_*$ the critical wave speed is negative and is well approximated by $c_c/Ra_c = -4.1 \times 10^{-3}\varepsilon$ (it can be shown that the specific constant is a function of Prandtl number and the dimensionless Sutherland constants). This result can be explained by inviscid

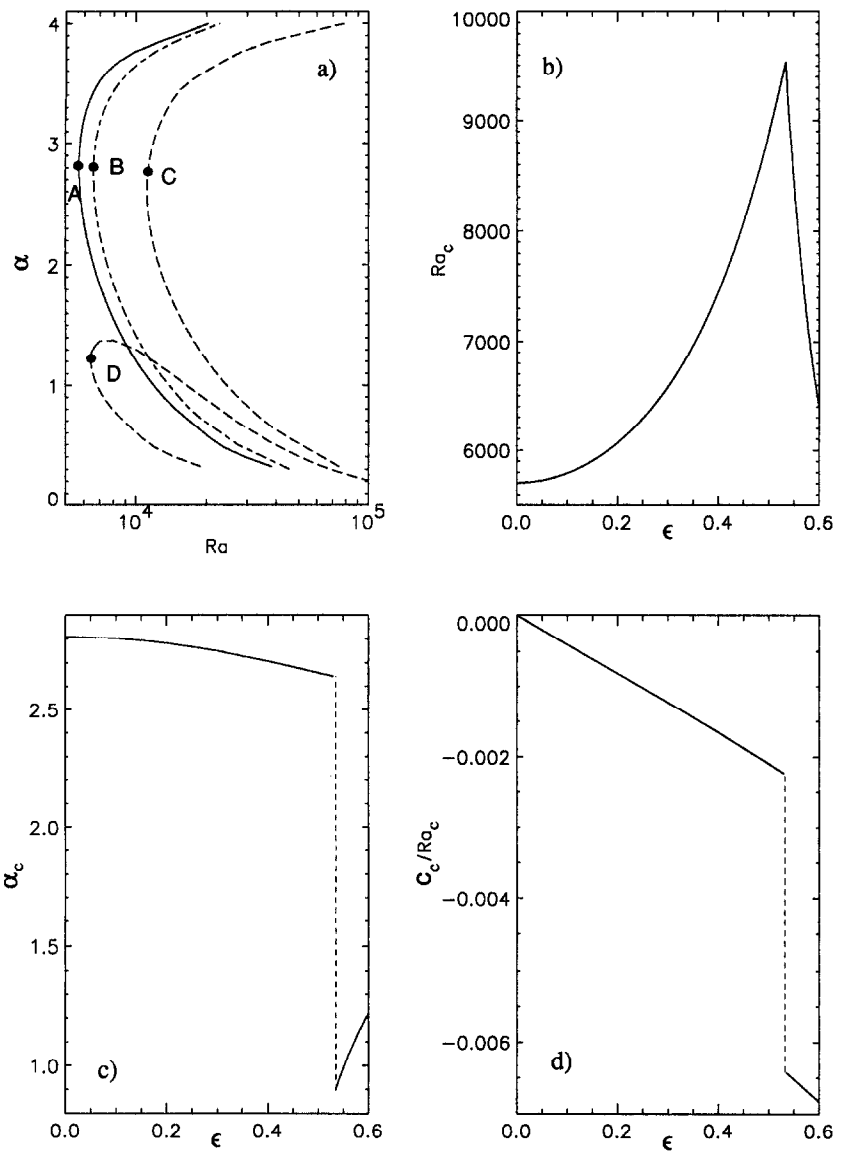

Fig. 2. (a) Marginal stability curves for $\varepsilon \ll 1$ (——), $\varepsilon = 0.3$ (— — —) and $\varepsilon = 0.6$ (- - - -) and (b)–(d) critical parameters as functions of ε.

stability theory as follows. Based on the numerical results for $Pr = 0.71$, it appears (see below) that this instability mechanism is shear driven and possibly linked to the presence of an inflection point in the basic velocity profile (see [19]). Indeed, it can be shown that in the limit $Pr \to 0$ equation (55) has a singularity at the location where the wave speed equals the basic flow velocity. This singularity is removable however (as it should be) if the basic flow velocity profile has an inflection point at the same location. This is exactly the same situation as in the Boussinesq limit. Note however that in the Boussinesq limit this singularity occurs at $x = 1/2$ where the basic velocity is zero and thus the wave speed is also zero; this location also corresponds to the location of the inflection point of the basic velocity profile. However, when properties in the basic flow are allowed to vary, the location of the inflection point and subsequently the location of the critical layer is given by

$$x_c = \tfrac{1}{2} + \frac{14 + 17S_k + 23S_\mu + 26S_kS_\mu}{60(1+S_k)(1+S_\mu)}\varepsilon + O(\varepsilon^3) \approx \tfrac{1}{2} + 0.29334\varepsilon \quad (59)$$

and the basic flow velocity at this location, and thus the wave speed, is given in this limit by

$$c_c = -\frac{Ra_c}{5760} f(S_k, S_\mu)\varepsilon + O(\varepsilon^3) \approx -2.63912 \times 10^{-3} Ra_c \varepsilon \quad (60)$$

where $f(S_k, S_\mu)$ is a positive definite function which

depends on the Sutherland constants and is too complicated to be given here. It is noted here that for $Pr > 0$, due to the contribution of viscous terms, the location of the critical layer is not the same as the location of the inflection point, but the two locations are found to be very close to each other. We stress the fact that the classical result that the instability is stationary for $Pr < 12.45$ is only due to the fact that *all* property variations are neglected. When property variations are included, the basic flow does not retain the odd symmetry about $x = 1/2$. Note that any mechanism which breaks the odd symmetry could possibly change the instability mechanism from stationary to oscillatory. In a study of instability in a differentially heated tall vertical annulus by Choi and Korpela [20] and Lee *et al.* [21] the odd symmetry was broken by the annulus curvature parameter. In their case a similar observation was made in that the instability was oscillatory for any finite value of the curvature parameter. However, the details are very different since in their case: the resulting wave speed is in the opposite direction as ours; the location of the critical layer does not coincide with the location of the inflection point of the basic flow; and lastly the parameter breaking the symmetry is a geometric one while in our case it is a physical one. A negative wave speed was also noticed by Simpkins [22] in his experiment on convection flow in a tall vertical cavity. He observed a slow downward motion of secondary rolls in a rectangular cavity of aspect ratio $A_H = 40$ for $\varepsilon \approx 0.15$ and $Ra \approx 6200$. The speed of motion he found is in close agreement with the value predicted by our calculations [23]. Consistent with (59), we also observe from the disturbance fields plotted in Figs. 4(a)–(d) that as ε increases the disturbance is located closer to the cold wall. At $\varepsilon \approx 0.475$ we first observe the appearance of a secondary branch at low wavenumbers in the marginal stability curve, and as ε is increased past ε_* the critical parameters switch to this lower branch. This switching at ε_* is responsible for the change in behavior of Ra_c and the abrupt changes in α_c and c_c seen in Figs. 2(b)–(d). We note that our values of the critical parameters in the Boussinesq limit are in excellent agreement with the values of $Gr_c^0 = 8037$ and $\alpha_c^0 = 2.81$ obtained by Chait and Korpela [24]. Furthermore, the result that the instability becomes oscillatory when property variations are accounted for is consistent with the results of Thangam and Chen [9] and Chen and Pearlstein [7].

To understand the physical mechanisms responsible for the two different modes of instability, we will look at the two-dimensional disturbance kinetic and thermal potential energy balances, $E_{KE} = \frac{1}{2}\langle\bar{\rho}(|u|^2 + |v|^2)\rangle$ and $E_{PE} = \frac{1}{2}\langle\bar{\rho}|T|^2\rangle$, respectively. Multiplying equation (47) by u^* and equation (48) by v^*, adding them together, and multiplying equation (50) by T^*, integrating them over the interval $0 \leqslant x \leqslant 1$, and taking the real parts we get

$$\sigma_R E_{KE} = \Sigma_\Pi + \Sigma_{uv} + \frac{RaPr}{2\varepsilon}\Sigma_B + Pr\Sigma_\mu \qquad (61)$$

$$\sigma_R E_{PE} = \Sigma_{Tu} + \Sigma_k \qquad (62)$$

where all the terms on the right-hand sides are defined in Appendix C. We see that the time rate of change of the disturbance kinetic energy $\sigma_R E_{KE}$ is the sum of contributions due to compressibility effects Σ_Π, productions due to shear Σ_{uv} and buoyancy $(RaPr/2\varepsilon)\Sigma_B$, and viscous dissipation $Pr\Sigma_\mu$, while the time rate of change of disturbance thermal potential energy $\sigma_R E_{PE}$ depends on the balance between the term Σ_{Tu}, which corresponds to the interaction between the basic flow temperature gradient and the perturbed velocity, and thermal diffusion Σ_k. The relative values for the different terms entering the disturbance kinetic energy equation for the critical points labeled A–D in Fig. 2(a) are presented in Table 1 (note that at these points $\sigma_R = 0$). Since the amplitude of the disturbance is arbitrary in a linear analysis, the normalization is done in such a way that $Pr\Sigma_\mu = -1$. In Fig. 3 we also present the distributions of the integrands of the disturbance kinetic energy equation correspondingly denoted by σ_Π, σ_{uv}, $(RaPr/2\varepsilon)\sigma_B$ and $Pr\sigma_\mu$. Note that the scales on the individual plots are arbitrary, thus one can only compare the relative energy contributions within each such plot. We can see that for Boussinesq and slightly non-Boussinesq regimes [corresponding to points A and B in Fig. 2(a)] the instability is a shear driven one, where the disturbance derives its energy from the shear of the basic flow which is largest near the center of the cavity. In addition we see that the maximum shear production always occurs near the location of the critical layer, i.e. the location where the disturbance wave speed is equal to the local basic flow speed. In cases where the instability is shear driven, as noted earlier, the critical layer is located very close to the inflection point of the basic flow, which in turn moves towards the cold wall as ε increases. We should also note the fact that compressibility effects do not contribute much to the disturbance kinetic energy balance in the integral sense in the weak non-Boussinesq regime (see Table 1, point B), but it does not mean that the disturbances are incompressible [see Fig. 3(b)]. When $\varepsilon > \varepsilon_*$ the disturbance derives the majority of its kinetic energy from the thermal interaction with the basic flow density field through buoyancy, hence resulting in a buoyant instability. The appearance of this new mode of instability is explained as follows. First we note that the local buoyancy contribution to the kinetic energy of the disturbance is given by

$$\frac{RaPr}{2\varepsilon}\sigma_B = RaPr\frac{1}{2}\frac{\bar{P}}{(1+2\varepsilon\bar{\theta})^2}(\theta v^*)_R \qquad (63)$$

where we have rescaled the temperature to remove the ε dependence from the boundary conditions by using the relation $\theta = (T^* - T_r)/(T_h^* - T_c^*) = (T-1)/2\varepsilon$ (so that $\bar{\theta} = \pm 1/2$ at $x = 0, 1$). Furthermore, we note that

$$\bar{P} = 1 - \frac{1}{6}\left(\frac{1-S_k}{1+S_k}\right)\varepsilon^2 + O(\varepsilon^4) \approx 1 - 3.55987 \times 10^{-2}\varepsilon^2 \qquad (64)$$

Table 1. Disturbance kinetic energy terms for the different values of critical parameters labeled A–D in Fig. 2

Point	Σ_Π	Σ_{uv}	$(RaPr/2\varepsilon)\Sigma_B$
A	0.0000	0.9418	0.0582
B	0.0008	0.9527	0.0465
C	−0.0020	0.9892	0.0128
D	−0.1448	0.4590	0.6858

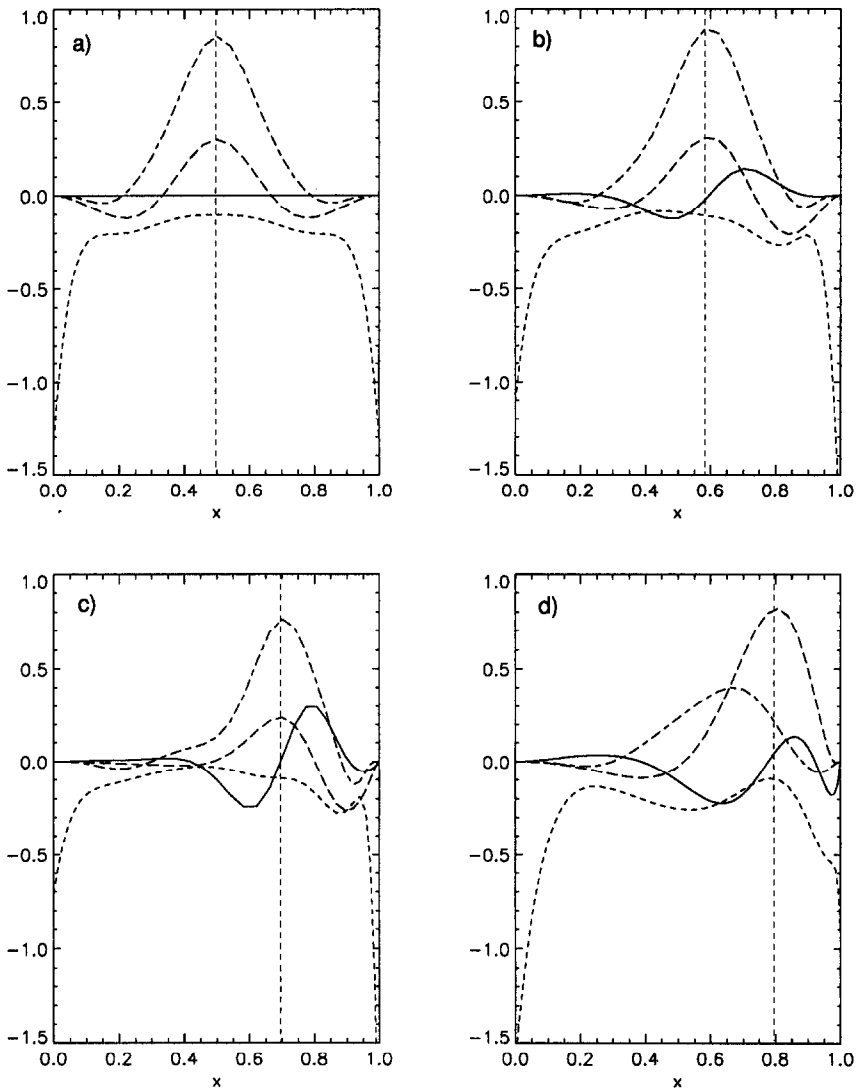

Fig. 3. Distributions of integrands appearing in the disturbance kinetic energy balance equation: σ_Π (———), σ_{uv} (——·——), $(RaPr/2\varepsilon)\sigma_B$ (----) and $Pr\sigma_\mu$ (. . .). Plots (a)–(d) correspond respectively to critical points A–D shown in Fig. 2(a). Vertical dotted lines denote locations of the critical layer.

and

$$\bar{\theta} = (\tfrac{1}{2}-x)+\frac{1}{2}\left(\frac{1+3S_k}{1+S_k}\right)x(1-x)\varepsilon+O(\varepsilon^2). \quad (65)$$

Now in the Boussinesq limit ($\varepsilon \to 0$) the buoyancy contribution becomes $RaPr\frac{1}{2}(\theta v^*)_R$. Since the shear contribution to the disturbance kinetic energy depends linearly with the Rayleigh number (through the basic flow dependence), then for fixed Prandtl number the ratio of the buoyancy contribution to that of the shear is always of the same order of magnitude, which numerically is seen to be small (see Table 1 for $Pr = 0.71$). On the other hand, when ε is finite the buoyancy contribution to the kinetic energy of the disturbance to leading orders in ε becomes

$$RaPr\frac{1}{2}\left\{\frac{1-\frac{1}{6}\left(\frac{1-S_k}{1+S_k}\right)\varepsilon^2}{1-2(2x-1)\varepsilon+\left[(2x-1)^2+2\left(\frac{1+3S_k}{1+S_k}\right)x(1-x)\right]\varepsilon^2}+O(\varepsilon^3)\right\}(\theta v^*)_R \tag{66}$$

which is largest in the vicinity of the cold wall since the term in brackets is largest at $x = 1$: however, both θ and v^* are zero there. The actual x-location where this term is largest depends on ε, S_μ, S_k and the specific disturbance correlation. We finally note now that for fixed Prandtl number the ratio of the buoyancy contribution to that of the shear can be increased by increasing ε. Thus the buoyancy contribution can be enhanced by either increasing the temperature difference for a specific fluid, or by varying the Prandtl number using different fluids for a fixed temperature difference. Ultimately, for fixed Prandtl number, at ε_* the buoyancy contribution becomes larger than that of shear and the mode of instability subsequently switches to a buoyant one. From the above discussion, the switch in mode of instability can be directly traced to the nonlinear density variation. As can be seen from equation (66), this nonlinearity in turn is due primarily to the nonlinear variation with temperature through the equation of state, and only secondarily through the variable conductivity. When the mode of instability becomes buoyant, we also note that global compressibility effects are significant, albeit stabilizing. In addition, as can be seen from Fig. 3(d) the location of the new critical layer corresponds to the location of maximum disturbance production due to buoyancy, which is closer to the cold wall than the location of the inflection point of the basic flow. Thus we conclude that the upper and lower marginal stability curves obtained for $\varepsilon = 0.6$, and shown in Fig. 2(a), obviously correspond to branches in which shear and buoyancy production dominate, respectively. The disturbance fields corresponding to the critical modes on these two branches are shown in Fig. 4. Note that the fields are shown for one wavelength, and their lengths are scaled by their corresponding critical values. Thus, the actual wavelength of the buoyant mode is more than a factor of two larger than the shear one. The change in mode of instability from one of hydrodynamic origin to one of thermal origin and the corresponding behaviors of the critical parameters are only superficially similar to those observed in the Boussinesq case [4] when the Prandtl number is increased past a value of 12.45. The two instabilities are not the same since in our problem the *local* Prandtl number is always less than unity and thus the source of instability is of a different nature.

We conclude this section with a few words regarding the sensitivity of the above stability results on the dimensionless parameters that up to this point we have fixed, i.e. Γ, S_k, S_μ and Pr. Since in all cases the instability occurs for $\alpha > 0$, then the results do not depend at all upon Γ. In addition, upon varying S_k and S_μ over reasonable values for gases, we observe that the qualitative stability picture remains the same, and quantitatively the results are only weakly affected. Lastly, as expected from the above discussions, the shear driven instability is only weakly affected by variation of Prandtl number. On the other hand, the buoyant instability is quantitatively sensitive to the Prandtl number. However, this sensitivity is fairly trivial since the local buoyant contribution to the kinetic energy of the disturbance is given by $(RaPr/2\varepsilon)\ \sigma_B$. Thus increasing the Prandtl number for fixed ε is approximately equivalent to quadratically increasing the magnitude of σ_B (through ε) for fixed Prandtl number. This correspondence establishes a relationship to the instability occurring in the Boussinesq limit for large Prandtl numbers. However, in contrast to our results, it should be noted that, in the Boussinesq case for $Pr > 12.45$, the instability sets in as two waves traveling in opposite directions on either side of $x = \frac{1}{2}$. Furthermore, since their wave speed is larger than the maximum speed of the basic flow, no critical layer exists.

6. CONCLUSIONS

We have examined the linear stability of the fully developed natural convection flow of air in a differentially heated tall vertical enclosure under non-Boussinesq conditions. The influence of the non-Boussinesq effects on the stability was studied over a large range of Rayleigh number and temperature difference. Our results are in excellent agreement with known results in the Boussinesq limit. In the non-Boussinesq regime we have shown that the mode of instability is controlled by a competition between the shear mechanism associated with the flow due to the temperature difference and a buoyancy mechanism (which becomes dominant only when $\varepsilon > 0.536$) that is clearly due to nonlinear density variations. Furthermore, while the critical wave speed is zero in the Boussinesq limit, for any finite value of ε the critical wave speed is negative, since, due to property variations, the location of maximum disturbance production shifts to the region close to the cold wall. This new result is in qualitative agreement with experimental data, reported in ref. [22].

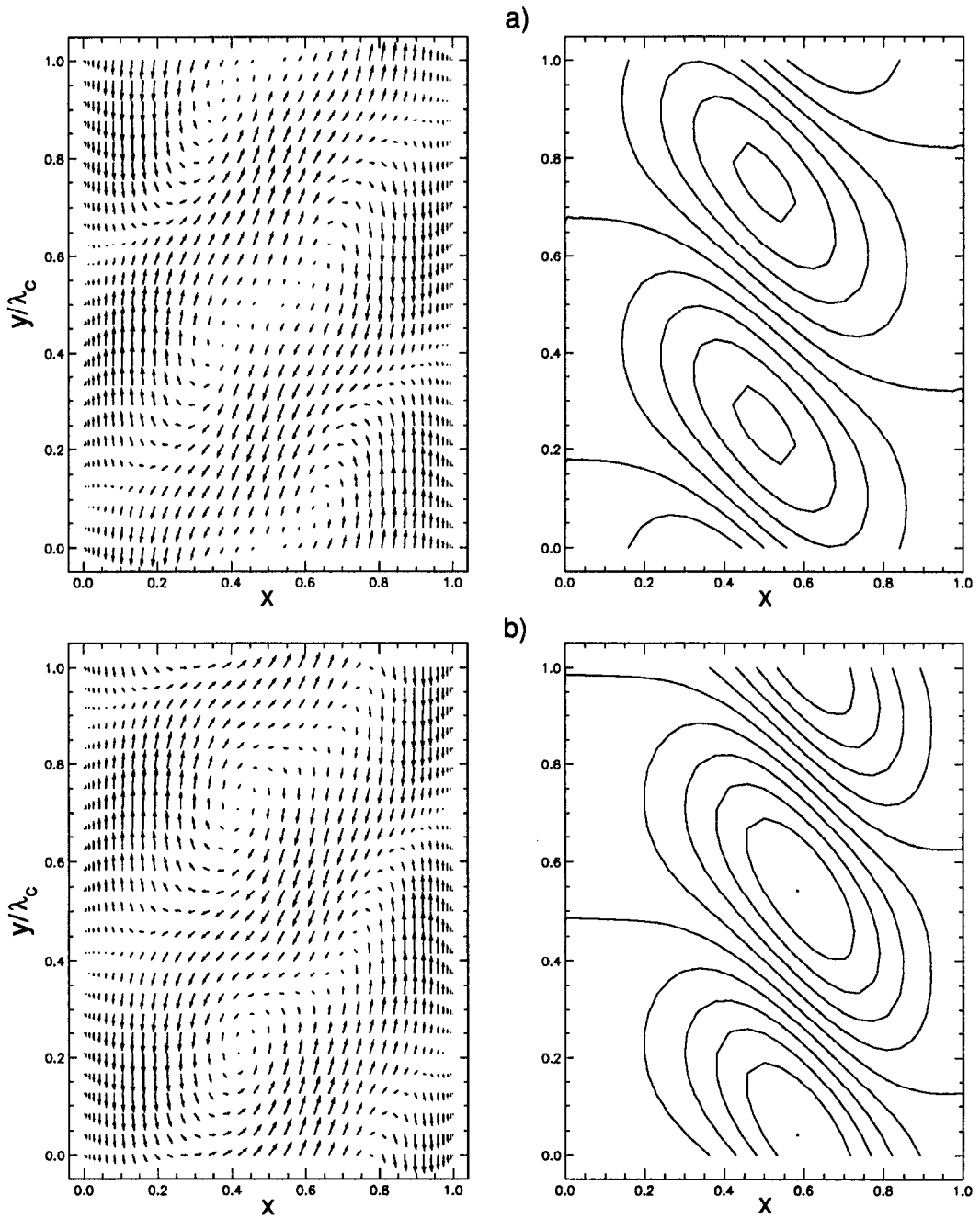

Fig. 4. Disturbance velocity field and isotherms for critical parameter values labeled (a) A, (b) B, (c) C and (d) D in Fig. 2. The vertical coordinates are normalized by their corresponding critical wavelengths $\lambda_c = 2\pi/\alpha_c$.

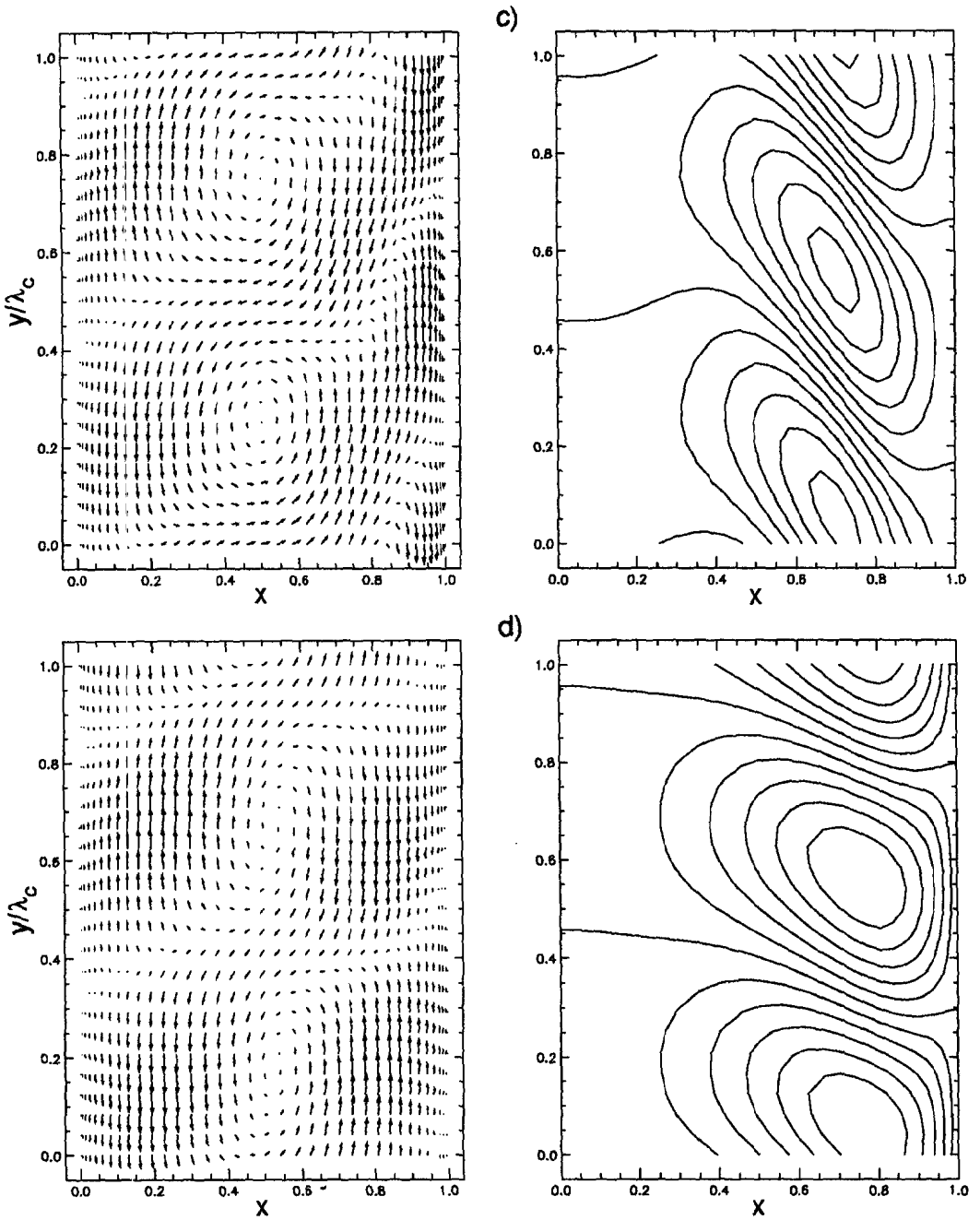

Fig. 4—*continued.*

Acknowledgement—The research reported in this paper has been partially supported by the Center for Applied Mathematics at the University of Notre Dame.

REFERENCES

1. R. N. Rudakov, Spectrum of perturbations and stability of convective motion between vertical plates, *Appl. Math. Mech.* **31,** 376–383 (1967).
2. C. M. Vest and V. S. Arpaci, Stability of natural convection in a vertical slot, *J. Fluid Mech.* **36,** 1–15 (1969).
3. J. E. Hart, Stability of the flow in a differentially heated inclined box, *J. Fluid Mech.* **47,** 547–576 (1971).
4. S. A. Korpela, D. Gözüm and C. B. Baxi, On the stability of the conduction regime of natural convection in a vertical slot, *Int. J. Heat Mass Transfer* **16,** 1683–1690 (1973).
5. R. F. Bergholz, Instability of steady natural convection in a vertical fluid layer, *J. Fluid Mech.* **84,** 743–768 (1978).
6. Y. Lee and S. A. Korpela, Multicellular natural convection in a vertical slot, *J. Fluid Mech.* **126,** 91–121 (1983).
7. Y.-M. Chen and A. J. Pearlstein, Stability of free-convection flows of variable-viscosity fluids in vertical and inclined slots, *J. Fluid Mech.* **198,** 513–541 (1989).
8. S. A. Suslov and S. Paolucci, Stability of mixed convection flow in a tall vertical channel under non-Boussinesq conditions, submitted to *J. Fluid Mech.* (1994).
9. *S. Thangam and C. F. Chen, Stability analysis on the convection of a variable viscosity fluid in an infinite vertical slot, Phys. Fluids* **29,** 1367–1372 (1986).
10. S. Paolucci, On the filtering of sound from the Navier–Stokes equations, Technical Report SAND82-8257, Sandia National Laboratories Report (1982).
11. F. M. White, *Viscous Fluid Flow*. McGraw-Hill, New York (1974).
12. D. R. Chenoweth and S. Paolucci, Natural convection in an enclosed vertical air layer with large horizontal temperature differences, *J. Fluid Mech.* **169,** 173–210 (1986).
13. D. D. Gray and A. Giorgini, The validity of the Boussinesq approximation for liquids and gases, *Int. J. Heat Mass Transfer* **19,** 545–551 (1976).
14. D. R. Chenoweth and S. Paolucci, Gas flow in vertical slots with large horizontal temperature differences, *Phys. Fluids* **28,** 2365–2374 (1985).
15. H.-C. Ku and D. Hatziavramidis, Chebyshev expansion methods for the solution of the extended Graetz problem, *J. Comp. Phys.* **56,** 495–512 (1984).
16. D. Hatziavramidis and H.-C. Ku, An integral Chebyshev expansion method for boundary-value problems of O.D.E. type, *Comp. Aths. Applic.* **11,** 581–586 (1985).
17. IMSL Mathematical Library, Version 1.1. IMSL Inc. Houston, TX (1989).
18. O. Vasilyev and S. Paolucci, Stability of unstably stratified shear flow in a channel under non-Boussinesq conditions, *Acta Mechanica*, in press.
19. C. C. Lin, *The Theory of Hydrodynamic Stability*. Cambridge University Press, Cambridge (1955).
20. I. G. Choi and S. A. Korpela, Stability of the conduction regime of natural convection in a tall vertical annulus, *J. Fluid Mech.* **99,** 725–738 (1980).
21. Y. Lee, S. A. Korpela and R. N. Horne, Structure of multicellular natural convection in a tall vertical annulus. In *Heat Transfer* 1982 (Edited by U. Grigull, E. Hahne, K. Stephan and J. Straub), Vol. 2, pp. 221–226 (1982).
22. P. G. Simpkins, Transition to periodic convective states in an air filled slot, *Bull. Am. Phys. Soc.* **34,** 2271 (1989).
23. P. G. Simpkins, Personal communications (1993).
24. A. Chait and A. Korpela, The secondary flow and its stability for natural convection in a tall vertical enclosure, *J. Fluid Mech.* **200,** 189–216 (1988).

APPENDIX A

The functions entering in the basic flow solution (25) and (26) are defined as follows in terms of $\tau = \sqrt{(\bar{T}/S_k)}$:

$$f(\tau) = \tfrac{1}{3}\tau^3 - F(\tau)$$

$$F(\tau) = \tau - \tan^{-1}\tau$$

$$\delta = 2(1+S_k)S_k^{3/2}$$

$$Q = \delta[f(\tau_c) - f(\tau_h)]$$

$$\theta(\tau) = (\tau^2 - \tau_h^2) + (S_\mu/S_k - 1)\ln\left(\frac{1+\tau^2}{1+\tau_h^2}\right)$$

$$\phi(\tau) = 2(\tau^5 - \tau_h^5)/15 + 2(S_\mu/S_k - 1)[f(\tau) - f(\tau_h)]/3$$

$$\omega(\tau) = [\tau^2 F(\tau) - \tau_h^2 F(\tau_h)] - [f(\tau) - f(\tau_h)] + 2(S_\mu/S_k - 1)\{[F(\tau) - G(\tau)] - [F(\tau_h) - G(\tau_h)]\} \quad \text{(A1)}$$

where

$$G(\tau) = \sum_{j=1}^{\infty} \frac{(-1)^{j+1}2^{2j}(2^{2j}-1)}{(1+2j)(2j)!} B_{2j}[\tan^{-1}\tau]^{1+2j}$$

and

$$B_{2j} = \frac{1}{(2j+1)2^{2j}}\left[2j - \sum_{n=1}^{j-1} 2^{2n}\binom{2n+1}{2n} B_{2n}\right]$$

are Bernoulli numbers generated for $j = 1, 2, 3, \ldots$ and

$$\binom{m}{n} = \frac{m!}{n!(m-n)!}$$

are the binomial coefficients. Subscripts h and c mean that the quantities are evaluated at $\bar{T} = T_h = 1+\varepsilon$ and $\bar{T} = T_c = 1-\varepsilon$, respectively.

APPENDIX B

The operators entering the eigenvalue problem (55) for $\alpha > 0$ are defined as follows using the fact that $D\bar{\mu} = \bar{\mu}_T D\bar{T}$ and $D\bar{k} = \bar{k}_T D\bar{T}$:

$$A_{11} = Pr\frac{1}{\bar{\rho}}\left[\bar{\mu}\left(\tfrac{4}{3}D^2 - \alpha^2\right) + \tfrac{4}{3}\bar{\mu}_T D\bar{T} D\right] - i\alpha\bar{v}$$

$$A_{12} = i\alpha Pr\frac{1}{\bar{\rho}}\left(\tfrac{1}{3}\bar{\mu}D - \tfrac{2}{3}\bar{\mu}_T D\bar{T}\right)$$

$$A_{13} = i\alpha Pr\frac{\bar{\mu}_T}{\bar{\rho}} D\bar{v}$$

$$A_{14} = -\frac{1}{\bar{\rho}} D$$

$$A_{21} = -D\bar{v} + i\alpha Pr\frac{1}{\bar{\rho}}\left(\tfrac{1}{3}\bar{\mu}D + \bar{\mu}_T D\bar{T}\right)$$

$$A_{22} = Pr\frac{1}{\bar{\rho}}\left[\bar{\mu}\left(D^2 - \tfrac{4}{3}\alpha^2\right) + \bar{\mu}_T D\bar{T} D\right] - i\alpha\bar{v}$$

$$A_{23} = Pr\frac{1}{\bar{\rho}}\left[\bar{\mu}_T(D^2\bar{v} + D\bar{v}D) + \bar{\mu}_{TT} D\bar{T} D\bar{v}\right] + \frac{RaPr}{2\varepsilon}\frac{1}{\bar{T}}$$

$$A_{24} = -i\alpha\frac{1}{\bar{\rho}}$$

$$A_{31} = -D\bar{T}$$

$$A_{33} = \frac{1}{\bar{\rho}}[\bar{k}(D^2-\alpha^2)+\bar{k}_T(D^2\bar{T} + 2D\bar{T}D)+\bar{k}_{TT}(D\bar{T})^2]-i\alpha\bar{v}$$

$$A_{41} = -\bar{P}D$$

$$A_{42} = -i\alpha\bar{P}$$

$$A_{43} = [\bar{k}(D^2-\alpha^2)+\bar{k}_T(D^2\bar{T}+2D\bar{T}D)+\bar{k}_{TT}(D\bar{T})^2]. \quad \text{(B1)}$$

APPENDIX C

The terms entering on the right-hand sides of the kinetic and thermal potential energy balances (61) and (62) are given by:

$$\Sigma_\Pi = \tfrac{1}{2}\langle\Pi(Du+i\alpha v)^*\rangle_R$$

$$\Sigma_{uv} = -\tfrac{1}{2}\langle\bar{\rho}D\bar{v}uv^*\rangle_R$$

$$\Sigma_B = \frac{1}{2}\left\langle\frac{\bar{\rho}}{\bar{T}}Tv^*\right\rangle_R$$

$$\Sigma_\mu = -\tfrac{1}{2}\alpha^2\left\langle\bar{\mu}\left(|u|^2+\tfrac{4}{3}|v|^2\right)\right\rangle - \frac{1}{2}\left\langle\bar{\mu}\left(\tfrac{4}{3}|Du|^2+|Dv|^2\right)\right\rangle + \tfrac{1}{2}\alpha\langle\bar{\mu}(uDv^*-u^*Dv)\rangle_I - \tfrac{1}{3}\alpha\langle\bar{\mu}(vDu^*-v^*Du)\rangle_I - \tfrac{1}{2}\langle\bar{\mu}_T D\bar{v}T(Dv+i\alpha u)^*\rangle_R$$

$$\Sigma_{Tu} = -\tfrac{1}{2}\langle\bar{\rho}D\bar{T}uT^*\rangle_R$$

$$\Sigma_k = -\tfrac{1}{2}\alpha^2\langle\bar{k}|T|^2\rangle - \tfrac{1}{2}\langle\bar{k}|DT|^2\rangle - \tfrac{1}{4}\langle\bar{k}_T D\bar{T}D(|T|^2)\rangle. \quad \text{(C1)}$$